Bulletin of Engineering Geology and the Environment (2021) 80:5091–5110
https://doi.org/10.1007/s10064-021-02215-4

ORIGINAL PAPER

Stress-dependence of the permeability, porosity, and compressibility in fractured porous media regarding fracturing condition

Parisa Bagherzadeh[1] · Kamran Goshtasbi[1] · Ezatallah Kazemzadeh[2] · Mojtaba Kashef[3] · Hessam Aloki Bakhtiari[2]

Received: 4 November 2020 / Accepted: 17 March 2021 / Published online: 11 April 2021

Abstract

Fractured reservoirs are important hydrocarbon resources. However, the production of hydrocarbon makes fractures to be sealed which in turn decreases the production rate. A better understanding of permeability, porosity, and compressibility of fractures would be useful in optimizing the production rate. This research paper explored stress-dependent permeability, porosity, and compressibility of fractured porous media, both experimentally and numerically. The laboratory results are used to calibrate numerical models. With this regard, the roles of fracturing parameters such as orientation, opening, fracture density, persistency, and the intersection of fractures on hydro-mechanical parameters of the fractured sample are analyzed individually. The results indicate that stress sensitivity of permeability and compressibility is more in fractured porous media than in non-fractured ones. The results gained also showed that samples with open fractures and no filling materials, dominant vertical fractures, and high fracture density have the most stress dependency of permeability and compressibility, while in high fracture densities, the fracture and matrix changes are close to each other. The intersection of joints and not persisted fractures act as obstacles. This causes the fluid to be trapped in porous media that affect reservoir recovery and increase financial losses. Finally, an analytical relationship is developed to calculate the matrix compressibility

Keywords Fractured reservoir · Compressibility · Permeability · Porosity · Laboratory tests · Numerical modeling

Introduction

Most fractured reservoirs behave as dual porosity-permeability systems, where the rock matrix and hydraulic fractures intricately contribute to hydrocarbon transport. While the natural fractures are open and secondary mineralization is very small, hydrocarbons move from the matrix to fractures in an unlimited way. Fluid moving speed from the matrix to fractures is controlled by the amount of pressure drop in fractures; the viscosity of the fluid flowing; matrix and fracture properties such as permeability, porosity, and compressibility; and fracture spacing (Lun et al. 2013). Although fractures make high initial rates, they tend to close by reservoir depletion. The fractures are much more compressible than the host rock. At initially overpressured reservoirs, the fracture closure is so considerable and results in small recovery and financial losses (Aguilera 1999).

The stress sensitivity studies have been done in different reservoir rocks. Theoretical and experimental studies on porous rocks' compressibility are investigated by Hall (1953), Newman (1973), Zimmerman et al. (1986), Zheng (1993),

✉ Parisa Bagherzadeh
p.bagherzadeh@modares.ac.ir

Kamran Goshtasbi
goshtasb@modares.ac.ir

Ezatallah Kazemzadeh
kazemzadehe@ripi.ir

Mojtaba Kashef
mojtaba.kashef@yahoo.com

Hessam Aloki Bakhtiari
bakhtiarih@ripi.ir

[1] Department of Mining Engineering, Faculty of Engineering, Tarbiat Modares University, Tehran, Iran

[2] Department of Petroleum Engineering, Research Institute of Petroleum Industry (RIPI), Tehran, Iran

[3] Department of Mining Engineering, Faculty of Engineering, University of Zanjan, Zanjan, Iran

Harari et al. (1995), Luo and Stevens (1996), Jalalh (2006a, b), Liu et al. (2009), Aloki Bakhtiari et al. (2011), and Moosavi et al. (2014). Also, porosity and permeability changes on shale samples are well documented by Soeder (1988), Dong et al. (2010), Ross and Bustin (2008), Ghanizadeh et al. (2014), Chen et al. (2015), Ma et al. (2016), Pan et al. (2015), Tan et al. (2017), Wang et al. (2016), and Zheng et al. (2016).

The influences of effective stresses on flow processes in fractured reservoirs are so crucial. Shale and coal reservoirs are considered fractured reservoirs which have low porosity and permeability and difficult for gas production. In this regard, Tan et al. (2019) reviewed laboratory methods and definitions to obtain fracture compressibility on coal and shale samples. They found that fracture compressibility is higher for coals than shales and also in non-proppant supported fractures. Furthermore, fracture compressibility is dependent on stress, gas type, and gas pressure. Permeability measurement tests on fractured shale samples under confining pressures from 5 to 80 MPa for simulating high effective stress in deep shale gas reservoirs were performed by Zhou et al. (2019). The permeability of fractured samples considerably decreases with effective stress. Based on fracture compressibility models, a stress-dependent fracture permeability model was extracted, while fracture compressibility is strongly stress-dependent. Coal fracture network evolutions by increasing effective stresses were investigated by in situ X-ray tomography apparatus (Zhang et al. 2019). Large fractures quickly compressed and porosity reduced considerably by the power law equation. Also, permeability decreased by one order of magnitude following an exponential function. By applying stresses, the fracture contact area increased and fracture compressibility decreased following both exponential and linear decreasing trends. The correlation between fracture permeability and effective stress for gas shales is investigated by Chen et al. (2015) through theoretical derivations. The fracture compressibility is an effective factor to correlate fracture permeability and effective stresses, while fracture compressibility is also dependent on initial fracture permeability, anisotropy, and mineral composition. Chen et al. (2016) has developed a unified permeability-effective stress relationship that can be applied to any type of fractured rock through theoretical derivation. Some authors of this work (Bagherzadeh et al. 2021) performed laboratory experiments on naturally fractured carbonate samples to study the effect of stress on permeability, porosity, and compressibility. Results indicate that stress sensitivity of permeability and compressibility in fractured reservoirs is strong; it means that fractures are much more compressible than the matrix. On the other hand, the stress sensitivity of porosity is much lower than permeability; fracture porosity is not so influenced by stress changes in fractured samples. Fracture closure and permeability reduction can be very notable at the initial production stage, leading to small recovery and financial losses. Lun et al. (2013) used artificial cores to evaluate the effect of fracture packing degree on stress sensitivity of permeability and porosity. The decrease in packing degree increases stress sensitivity of permeability. Carvajal et al. (2010) conducted a series of laboratory tests on weakly anisotropic micro-fractured sandstones, where rock compressibility was measured in different stress paths and fracture density. Fracture density has a significant effect on stress sensitivity and the initial value of rock compressibility. Abass et al. (2007) conducted a series of experiments to assess the stress-dependent permeability of matrix, natural fractures, and hydraulic fractures as a function of various combinations of effective stress. The experiment results indicate that tensile fractures have much less hydraulic conductivity than shear fractures and the shear fractures have less hydraulic conductivity than propped ones. Fracture aperture is often constant during production, while Pinzon et al. (2000), by considering some field data, have shown that the permeability of naturally fractured reservoirs declines by production and pressure depletion. Meanwhile, Dwi et al. (2007) found that hydraulic conductivity increased due to production from naturally fractured reservoirs and indicated that pressure drop in reservoir results in fracture slide and increasing fracture permeability in critical stress condition. Haifeng et al. (2015) have proposed a scaled model simulating several parallel fractures in low permeability reservoirs. In a scaled model, the influence of parameters such as sample size, groundwater flow rate, fracture density, fracture permeability, and in situ stresses is considered. Tao et al. (2009) used the poroelastic displacement discontinuity method and fully coupled fracture change with pore pressure in matrix and fractures to investigate stress dependency of fracture aperture and permeability. Increasing effective normal stress decreases fracture permeability by production. Also, the fracture permeability is not always reduced by pressure depletion and could be enhanced by production in high anisotropic stress conditions, where fractures are very weak to shear deformation.

Due to the importance of stress effect on reservoir performance, especially fractured reservoirs, different studies by considering various assumptions and laboratory conditions have been performed. In this study, using laboratory experiments and numerical simulation, the stress effects on permeability, porosity, and compressibility of fractured carbonate rocks are investigated simultaneously, which are not explored yet. Three dimensional fully hydro-mechanical coupling models by considering the effect of fluid flow from the matrix to fractures were used for modeling. The effects of fracturing parameters such as fracture orientation, opening, density, and persistency on hydro-mechanical parameters of porous media are discussed separately and conformed to laboratory results. An analytic relationship is also developed for estimating matrix compressibility which can separate fracture and matrix compressibility values. This research paper is a useful reference for predicting reservoir behavior in

different fracturing conditions in the production stage from naturally fractured reservoirs.

Methodology

A series of experimental studies and numerical modeling were used to exploit fluid flow in fractured porous media. Naturally fractured samples are tested using the CMS-300 apparatus. Samples are categorized into A, B, and C classes, regarding fracture existence and orientation. Porosity, permeability, and compressibility have been measured at eight effective stresses, and the importance of fracture orientation, opening, density, and intersection on poroelastic parameters of fractured porous media is discussed.

Due to natural sample complexity and the combination of different factors that affect experimental results, a sensitivity analysis using numerical simulation has been done. Sensitivity analysis has been performed to consider the effect of each fracturing parameter individually, such as fracture orientation, density, opening, and persistency on poroelastic parameters. In this regard, a three-dimensional distinct element coupling code has been developed to study fluid flow through matrix and fractures. The flow in the matrix is coupled to the flow in joints as the fluid in the joints can flow into the surrounding matrix. Also, the fluid flow in rock masses is a hydro-mechanically coupled problem where fluid pressure affects the mechanical deformation, and mechanical deformation affects pressures. The code also is verified by laboratory experiments.

Laboratory experiments

The stress dependency of permeability, porosity, and compressibility of fractured porous medium considering fracturing conditions is evaluated under increasing confining pressures.

Experimental setup and procedure

In this study, cylindrical fractured carbonate rock samples were recovered from a specific well in Iran's south oil basin. Plug dimension is 38 mm (1.5 in.) diameter and 50.8 mm (2 in.) height. Samples were washed with toluene and methanol using a Soxhlet extraction apparatus to ensure that porous space was free of salts, drilling mud, and petroleum products. Before determining the rock's petrophysical properties, the samples are dried in an oven at 60 °C for 24 h. After washing and drying the cores, the permeability and porosity of the matrix were measured in ambient conditions. Porosity is measured using helium gas expansion and Boyle's law, and rock permeability is measured using air permeability meter based on Darcy's law. The results are shown in Table 1.

CMS-300 apparatus has been used to measure pore volume compressibility, porosity, and permeability in different effective stress intervals by helium injection into the core plugs. CMS-300 can measure pore volume compressibility and calculate porosity and permeability at different hydrostatic stress conditions. Porosity and pore volumes were obtained from the apparatus at each effective stress increasing intervals. Porosities were measured by injection of Helium gas that applies Boyle's law, where the helium gas from the reference cell is isothermally expanded to the sample cell. Then, equilibrium pressure is measured to obtain porosity. Klinkenberg permeability of all samples is measured simultaneously. In this study, the maximum stress value has been set to 4000 psi, and stress has changed at eight ascending steps discontinuously; the stresses are 3.44, 5.17, 6.9, 10.34, 13.78, 17.24, 20.68, and 27.5 MPa. Samples are classified into A, B, and C categories, based on fracture existence and orientation. Type A is a non-fractured specimen with low porosity and permeability; type B is a vertical core that illustrates horizontal fractures perpendicular to the sample axis. Type C is horizontal cores that express vertical fractures parallel to the sample axis.

Since sample appearance does not clearly illustrate fracture and matrix arrangement, microscopic CT scan images are used to reveal fracturing conditions. Due to the high accuracy and resolution of the CT scanner (300 microns), images were taken at 0.1 mm intervals so that more than 700 images were taken from each sample which has 1.5 * 2 in. dimensions. Using CT scan image processing software, the fracturing condition can distinguish. One longitudinal section in 18 mm of sample diameter and three cross sections of CT scan images in 13, 25, and 36 mm length intervals are shown in Fig. 1.

The matrix is dense without significant changes in the rock microstructure. White veins of marl are seen through this silty-clayey carbonate rock. Specimen type A (V111) is non-fractured; type B (V2) has horizontal fractures with oblique micro-fractures along the sample, while dominant fractures are horizontal; and type C has vertical fractures with different opening and placement. Initial porosity and permeability values are shown in Table 1, displaying a general overview of fracturing conditions. For example, the H33 sample has maximum permeability, i.e., $8.685*10^{-14}$ m^2. From CT scan images, H33 has two open fractures extended through sample length. Maximum porosity values are observed in H2 and V2 specimens, while V111, a non-fractured sample, has the lowest porosity and permeability.

Experimental results

In this section, based on laboratory investigations, the effects of stress on permeability, porosity, and compressibility of fractured carbonate rocks are discussed. The experiments conducted while confining stress discontinuously increased in eight steps, from 3.44 to 27.5 MPa. Permeability, porosity, and compressibility curves are shown in Fig. 2a–c.

Table 1 Specimen's parameters in ambient condition

Sample no.	V111	V2	H23	H33	H22	H31	H2	H47	H36	H8	H14
Sample type	A	B	C	C	C	C	C	C	C	C	C
Weight (gr)	141.5	131.3	136.4	135.7	138.65	137.3	130.5	138.3	135.9	137.5	139.1
Length (cm)	5	5	5	5	5.1	5	5	5	5	4.5	5
Diameter (cm)	3.8	3.8	3.8	3.8	3.8	3.8	3.83	3.83	3.81	3.85	3.86
Grain density (gr/cc)	2.7	2.54	2.5	2.57	2.59	2.62	2.6	2.5	2.6	2.49	2.53
Initial porosity (%)	8.5	14	9.31	11.52	10.3	10.8	15	9	10.6	13.5	9.8
Initial permeability (m^2)*10E-16	1.08	3.45	9.37	868.5	35.53	43.92	8.88	8.88	5.62	35.5	5.03

Figure 2a indicates that the non-fractured sample, V111, has the lowest initial permeability. By increasing stress due to the closure of pores and connected spaces, permeability value has reduced by 27% at 27.5 MPa. However, stress-dependent permeability is much lower than fractured specimens.

The fractures of type B (V2) specimen are perpendicular to the flow path and sample axis. Initial permeability is only higher than type A, the non-fractured one. However, as soon as applying stress, the permeability drops, so the lowest permeability has occurred at 27.5 MPa, and it reduces by 98%. Although the flow path and fracture direction are perpendicular to each other, the existence of some oblique fractures makes a route for passing the fluid and fracture compression.

Type C specimens with vertical fractures parallel to the sample axis and flow path have more initial permeability than types A and B. Stress-dependent permeability is evident in all type C samples, while permeability has reduced from 80 to 98%. It is realized that the stress sensitivity of permeability in fractured samples is higher than the non-fractured ones.

By applying confining stresses, porosity values are reduced in a smooth slope (Fig. 2b). Porosity reduction in type A, which represents the rock matrix, type B, and type C specimens is 6%, 7%, and 3–6%, respectively. It means that the effect of stress on porosity is less than permeability in fractured specimens.

Also, compressibility versus effective stress is shown in Fig. 2c. Compressibility reduction in fractured specimens is 85%, which is higher than V111, a non-fractured one.

The laboratory results in fractured specimens indicate influential role of fracturing conditions, including fracture orientation, opening, persistency, and fracture density. Due to the complexity of natural samples and the combination of several effective factors on poroelastic parameters of porous media, these parameters are discussed separately through numerical simulation, which is verified and compared with laboratory results.

Numerical modeling of hydro-mechanical behavior of natural rock fractures

The software used for the numerical calculations is the 3DEC code based on the distinct element method formulation. The flow in the matrix has coupled to the flow in the joints, while the fluid in joints can flow into the surrounding matrix. Fluid flow in rock masses is a hydro-mechanically coupled problem where fluid pressure affects mechanical deformation and mechanical deformation affects pressures.

The governing equations for fluid flow in joints follow a simplified form of the Navier-Stokes equation. For hydro-mechanical analysis and fluid flow calculations, the discontinuity geometrically conformed to a two-dimensional flow plane. Fluid flow occurred along the discontinuity plane while the intact surrounding material is impermeable. The flow rate per unit width of discontinuity is estimated by the "modified" cubic law (Itasca (2013)):

$$q = -\frac{u_h^3 \rho g}{12\mu}\nabla_h = -K_h \nabla_h \tag{1}$$

where u_h is the equivalent hydraulic aperture of the idealized fracture (m), k_h is the hydraulic conductivity of the fracture (m/s), ∇_h is the hydraulic gradient, ρ is the fluid density (kg/m^3), g is the gravitational acceleration (m/s^2), and μ is the fluid dynamic viscosity (Pa s). The value of hydraulic aperture is calculated in the elastic range and updated as a function of the effective normal stress:

$$u_h = u_{h0} + f\frac{\Delta\sigma_n^{'}}{K_n} \tag{2}$$

where u_{h0} is the initial hydraulic aperture, $\Delta\sigma_n^{'}$ is the effective normal stress variation, and f is a factor that describes the roughness influence. Fracture walls are planar, while factor f is 1 in 3DEC.

Normal and shear joint stiffness is explained by linearly elastic springs. The Coulomb slip law characterizes the shear resistance of the joint.

For fluid flow simulation within joints, the hydraulic aperture of fracture varies as a linear function of normal stress, σ_n, and it is controlled by the normal displacement of fracture Δu_n given in Eq. (3) (Itasca (2013)):

$$u_h = u_{h0} + \Delta u_n \tag{3}$$

where u_{h0} is the joint aperture in zero normal stress and u_h is the joint normal displacement (positive denoting opening). U_{res} is the minimum (residual) value for the joint aperture,

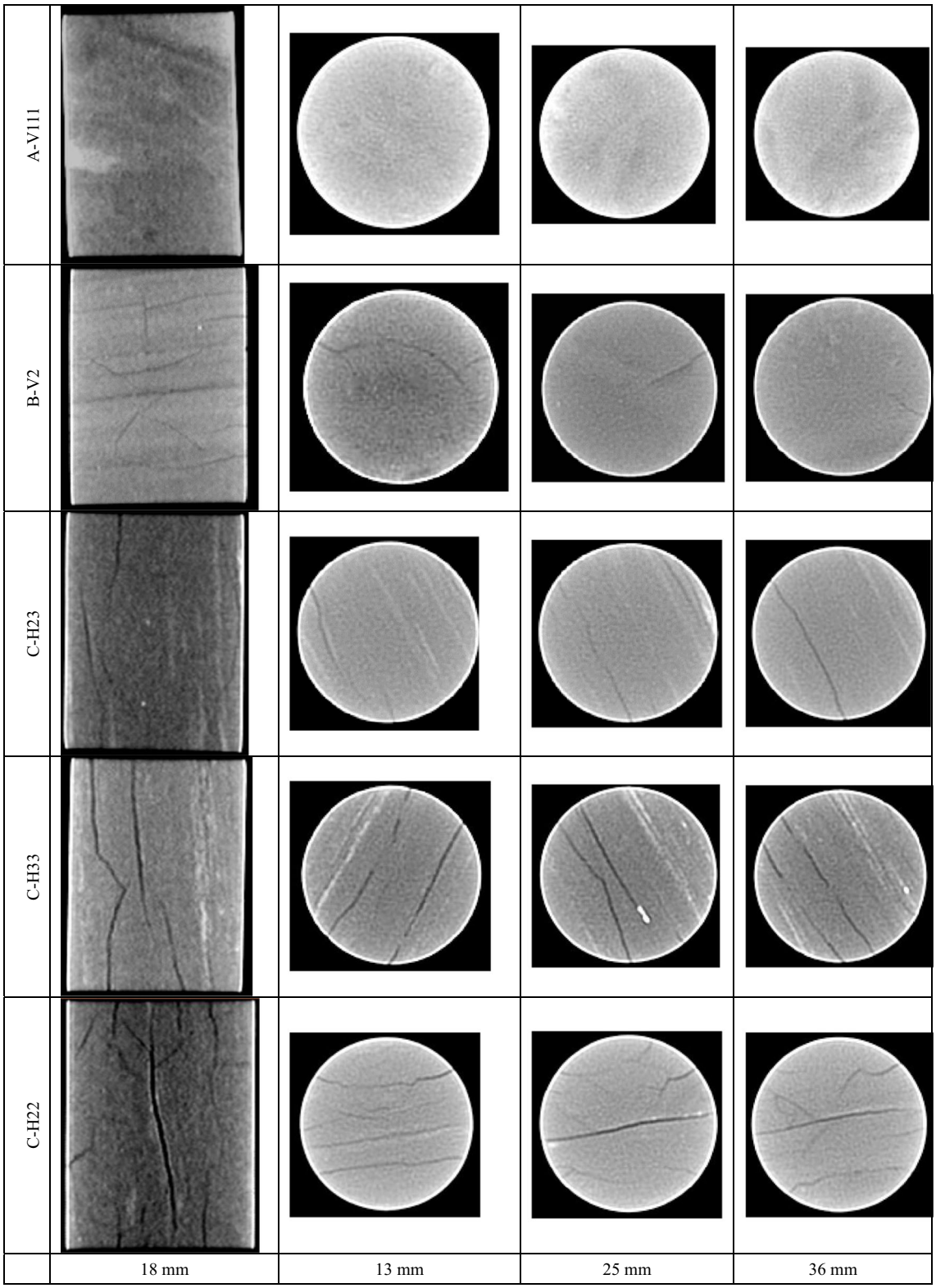

Fig. 1 Computed tomography images of laboratory samples in a longitudinal section (18 mm) and three cross sections (13, 25, and 36 mm) of the sample

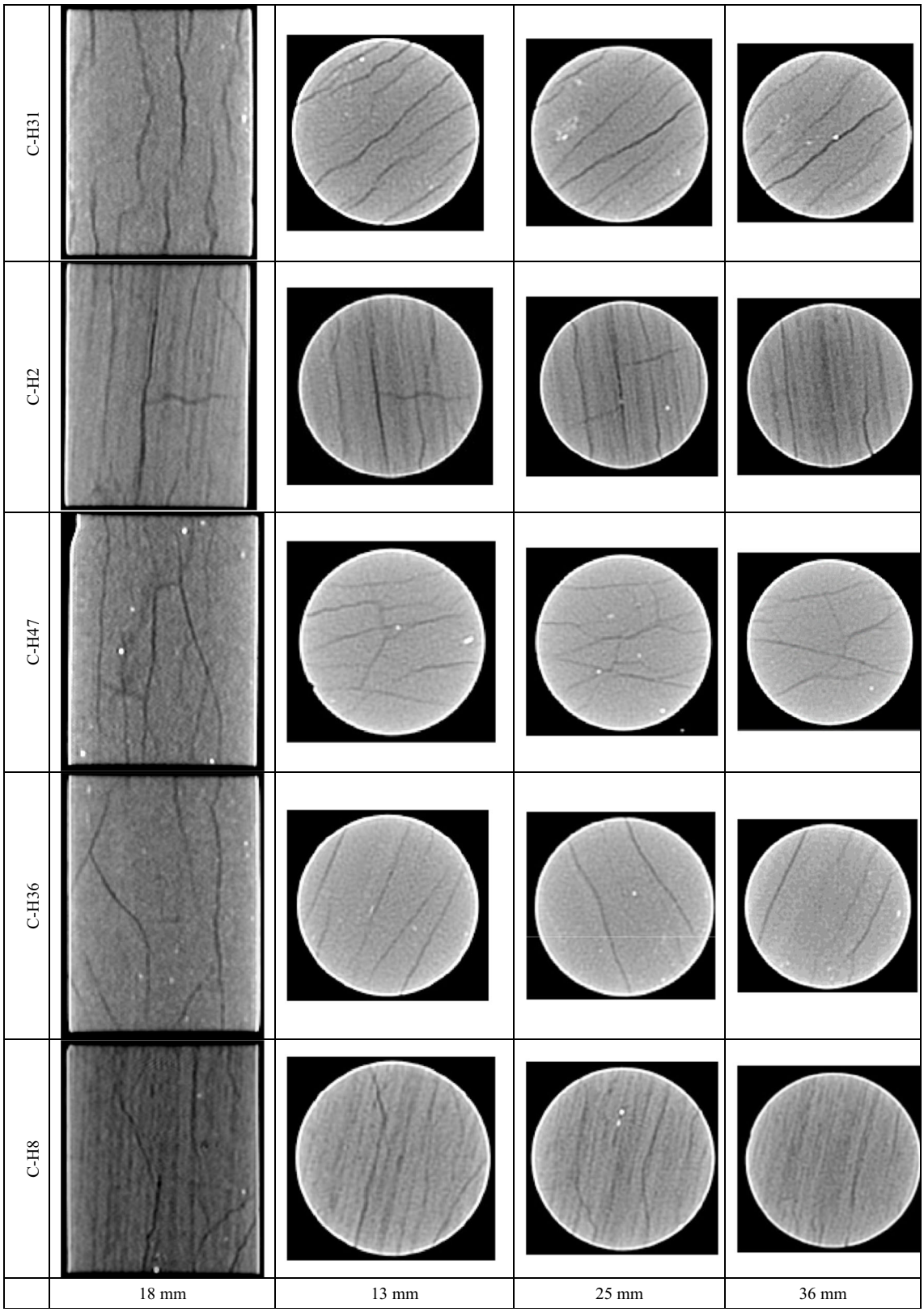

Fig. 1 continued.

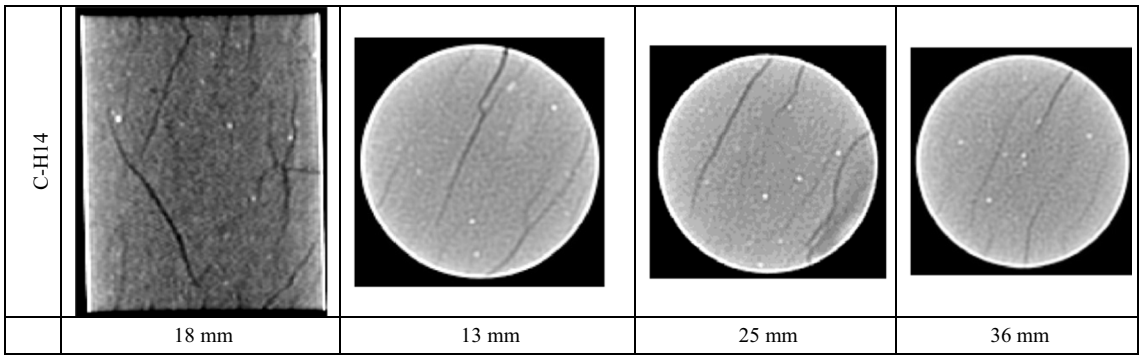

Fig. 1 continued.

below which the contact permeability is not affected by mechanical closure. U_{max} is the maximum value uses in flow rate calculation assumed for efficiency in the explicit calculation.

Pressures are calculated and stored in a data structure called a flow-knot. Flow rate and flow-knot pressures are updated. The new flow-knot pressure becomes

$$p = p_0 + K_w Q \frac{\Delta t}{V} - K_w \frac{\Delta V}{V_m} \tag{4}$$

where p_0 is the flow-knot pressure in the preceding time step; Q is the sum of flow rates into the flow-knot from all surrounding contacts; and K_w is the bulk modulus of the fluid.

$$V = V - V_0 \tag{5}$$

$$V_m = (V + V_0)/2 \tag{6}$$

V and V_0 are the new and old flow-knot volumes, respectively. To run a coupled solution, both mechanical and flow mode must be on. Internally, 3DEC runs a series of mechanical steps, followed by a series of fluid steps (Itasca (2013)).

Cylindrical samples were modeled in hydrostatic stress condition that is the mechanism of the CMS-300 apparatus. The sample is drained from the outlet, and no shear or slip occurs on matrix and fractures.

The initial stress state is isotropic, and lateral pressure is kept constant during the test, the base of the model is fixed in the axial direction, and an axial velocity is applied at the top of the model. The boundaries are impermeable; also, all grid points are initially "free," which means that pore pressure at such knots is free to vary according to the net inflow and outflow from neighboring zones. The pore pressure is fixed at the end of the sample to let the fluid leave the external boundary from the outlet.

Figures 3 and 4 have shown the direction of discharge vectors in the matrix (a) and fracture (b) at the initial and final stages of loading. As the pressure increases, the fluid is discharged simultaneously through the fractures and the matrix. At the initial stages of loading, production from the fractures is only ten times greater than the matrix. But in the final stages of applying pressures, the amount of discharge is 100 times greater than the matrix. It proves that fractures have a crucial role in the reservoir production.

Analytic relationships for measuring hydro-mechanical parameters

As CMS equipment measures total poroelastic parameters and do not distinct fracture and matrix values, analytical relations are developed to measure matrix and fracture parameters individually. Fracture aperture calculated and updated in 3DEC software, so fracture compressibility, C_f, is obtained using Eq. (7), where b is the aperture and b_0 is the initial aperture at reference pore pressure.

Fracture porosity and permeability are estimated using Eqs. (8) and (9) (Chacon, 2006), where $\varnothing_{fi}$ and K_{fi} are initial fracture porosity and permeability and $\varnothing_f$ and K_f are current fracture porosity and permeability.

$$C_f = \frac{-\ln \frac{b}{b_i}}{P_{pi} - P_p} \tag{7}$$

$$\phi_f = \phi_{fi} e^{-c_f (Ppi - Pp)} \tag{8}$$

$$K_f = K_{fi} e^{-3c_f (Ppi - Pp)} \tag{9}$$

Therefore, porosity, permeability, and compressibility of fractures are measured. In the saturated matrix, pore volume changes equal the variation of fluid volume trapped in pore space, i.e., $\Delta V_p = \Delta V_f$. So fluid volume ΔV_f changes can decompose into two parts as Eq. (10) (Detournay and Cheng 1993):

$$\nabla V_f = \Delta V_f^{(1)} + \Delta V_f^{(2)} \tag{10}$$

$\nabla V_f^{(1)}$ is the component associated with the compression or dilation of the interstitial fluid, and $\nabla V_f^{(2)}$ is the component due to fluid exchange between the porous material and the

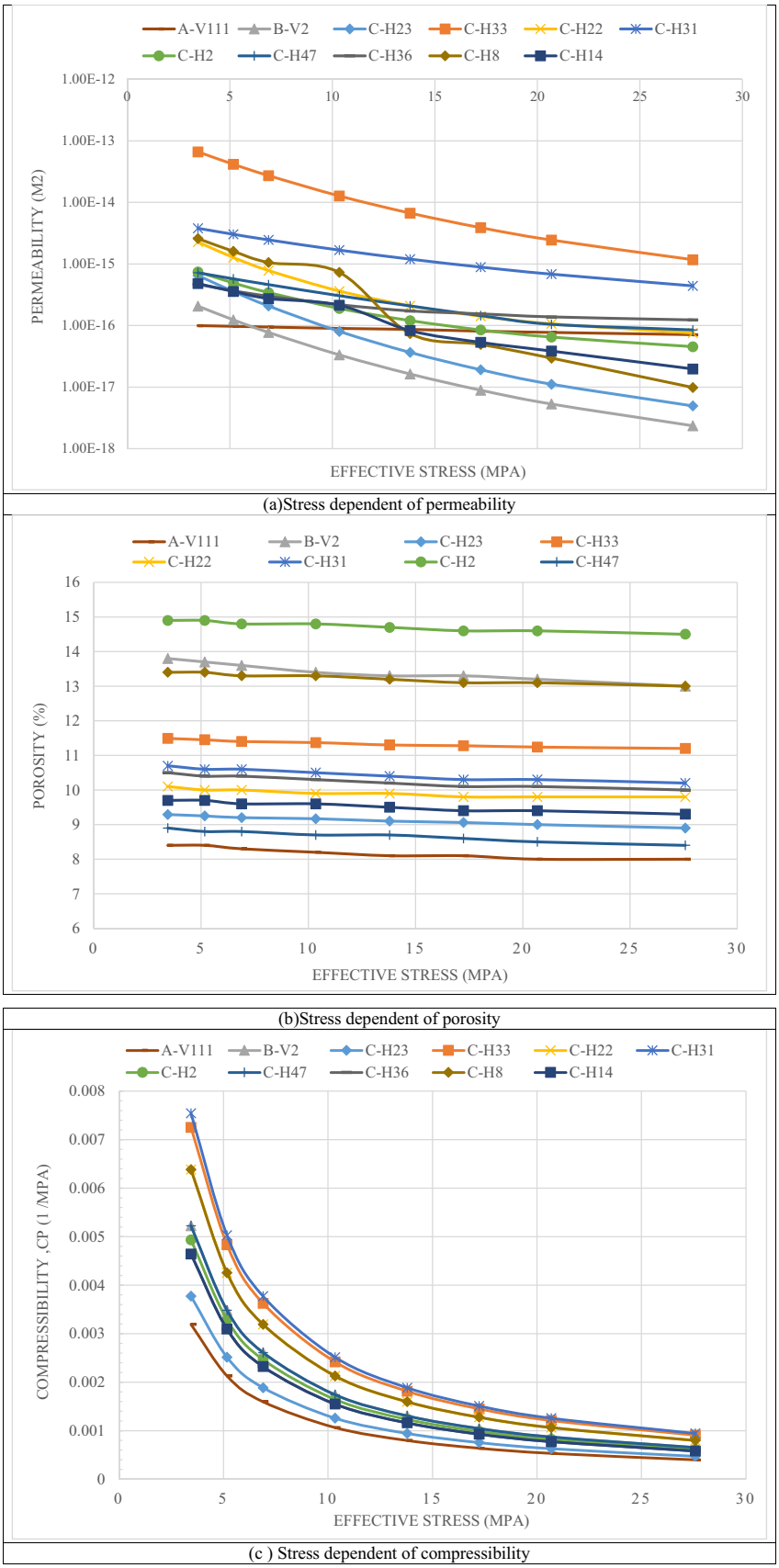

Fig. 2 Stress-dependent **a** permeability, **b** porosity, and **c** compressibility of carbonate samples, type A (without fracture), type B (horizontal fracture), and type C (vertical fractures)

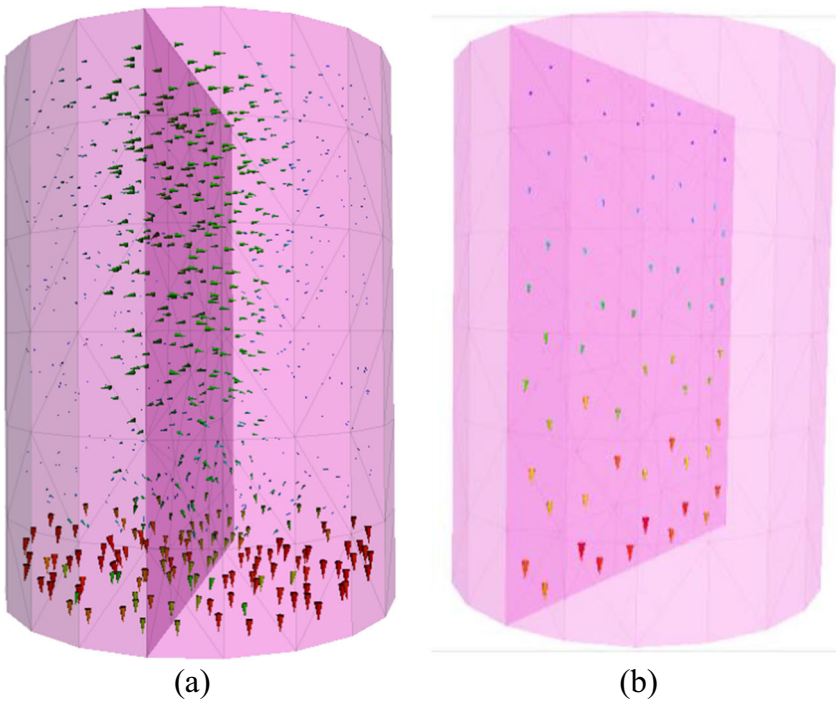

Fig. 3 Discharge vectors at initial stages of loading in **a** matrix and **b** fracture

outside. $\nabla V_{\mathrm{f}}^{(1)}$ expresses pore pressure p, as Eq. (11), where K_{f} is the fluid bulk modulus.

The second component $\nabla V_f^{(2)}$ is related to the variation of fluid content ζ introduced by Eq. (12). A constitutive relation can be derived for ζ in Eq. (13). P and p are confining stress and pore pressure, α is Biot coefficient, K_p is bulk modulus for the pore volumetric strain, and B is the Skempton pore pressure coefficient that is 1 for incompressible fluid, and compressible fluid is obtained by Eq. (14) (Detournay and Cheng 1993).

$$\frac{\Delta V_f^{(1)}}{V_f} = -\frac{p}{K_f} \tag{11}$$

$$\zeta = \frac{\Delta V_f^{(2)}}{V} = \frac{\phi \Delta V_f^{(2)}}{V_f} \tag{12}$$

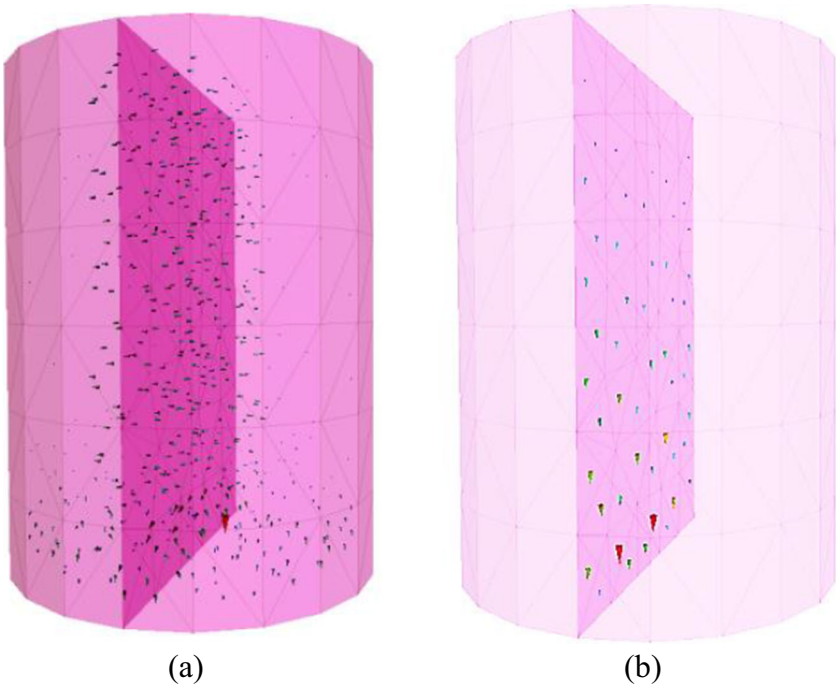

Fig. 4 Discharge vectors at final stages of loading in **a** matrix and **b** fracture

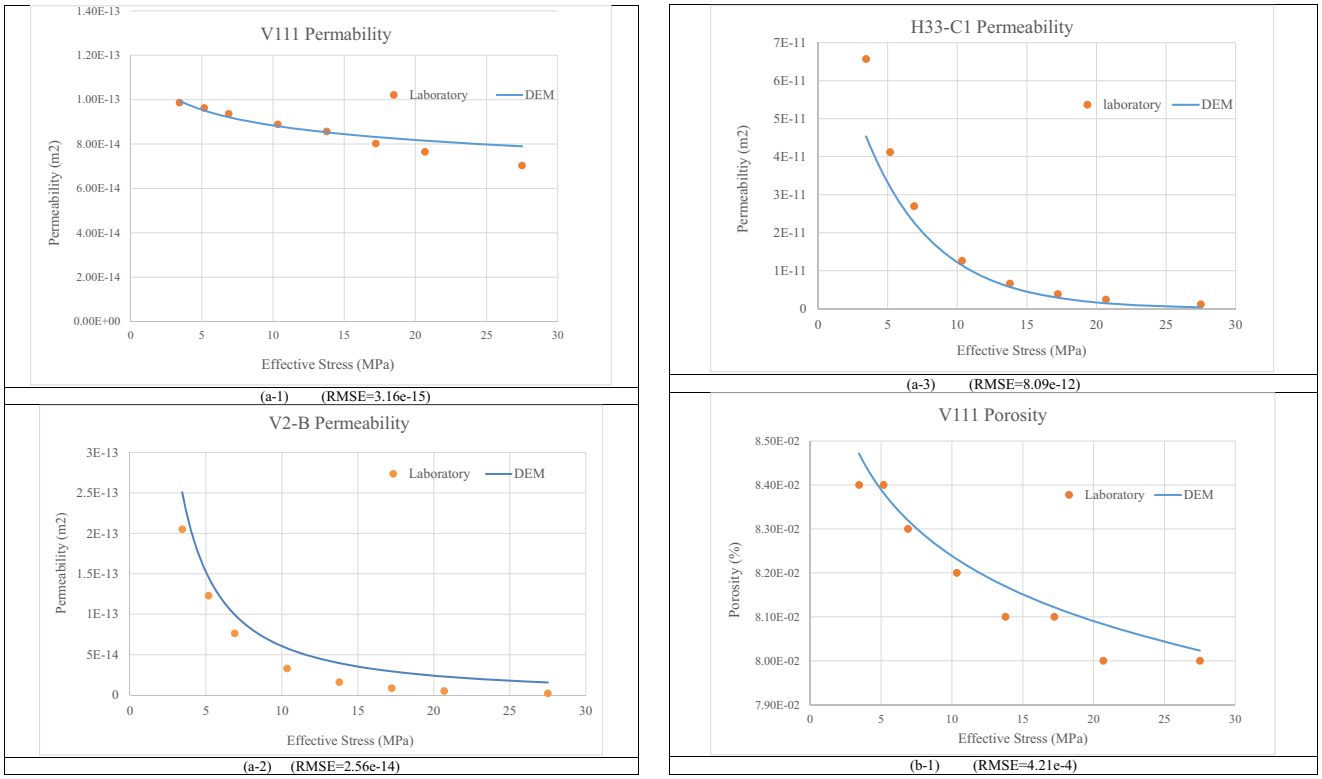

Fig. 5 Verifying numerical modeling with laboratory data in A-V111, B-V2, and C1-H33 samples: **a** permeability, **b** porosity, and **c** compressibility

$$\zeta = -\frac{\phi}{K_p}\left(P - \frac{p}{B}\right) \tag{13}$$

$$B = \frac{\alpha K_f}{\varnothing K} \tag{14}$$

Using Eqs. (11), (13), and (10) is written as Eq. (15):

$$\frac{\nabla V_f}{V} = \frac{\nabla V_f{}^{(1)}}{V_f} + \frac{\Delta V_f^{(2)}}{V} = -\frac{p}{k_f} - \left[\frac{\varnothing}{K_p}\left(P - \frac{p}{B}\right)\right] \tag{15}$$

Therefore, Eq. (15) can be written in the form of Eq. (16):

$$\frac{\nabla V_f}{V} = -\frac{p}{k_f} - \left[\frac{\alpha}{K}\left(P - \frac{pK\varnothing}{\alpha K_f}\right)\right] \tag{16}$$

Using Eq. (11), matrix compressibility is obtained as Eq. (17):

$$C_{pc,m} = \frac{\nabla V_f}{V}/\nabla P \tag{17}$$

Equation (17) has developed in numerical modeling for calculating matrix compressibility. Also, fracture compressibility has acquired using Eq. (7). Total compressibility is the summation of matrix and fracture compressibility obtained as Eq. (18):

$$C_{pc\ (f+m)} = C_{pc\ (f)} + C_{pc(m)} \tag{18}$$

Numerical results

Because of natural sample complexity and several factors combination that affect experimental results, the parameters are explored individually by sensitivity analysis via numerical simulation. Studied parameters are fracture orientation, aperture, density, persistency, and intersection. Before investigating the sensitivity analysis obtained by numerical simulations, numerical results should be verified using laboratory experiments. In this regard, samples from type A-V111, type B-V2, and type C-H33 were used for calibration. Figure 5a–c show porosity, permeability, and pore volume compressibility curves versus effective stress by numerical modeling and laboratory experiments. A suitable correlation was found between obtained factors from numerical analysis (blue line) and laboratory investigations (orange points). RMSE value shows the difference between tested and predicted values through numerical simulation.

Fracture orientation effect on permeability, porosity, and compressibility

The effect of fracture orientation is explored in samples with parallel fractures and 0.3 mm opening. Fracture direction is examined at 0, 10, 20, 30, 40, 50, 60, 70, 80, and 90 degrees. Permeability, porosity, and compressibility of fractures relative to effective stress are shown in Fig. 6a–c.

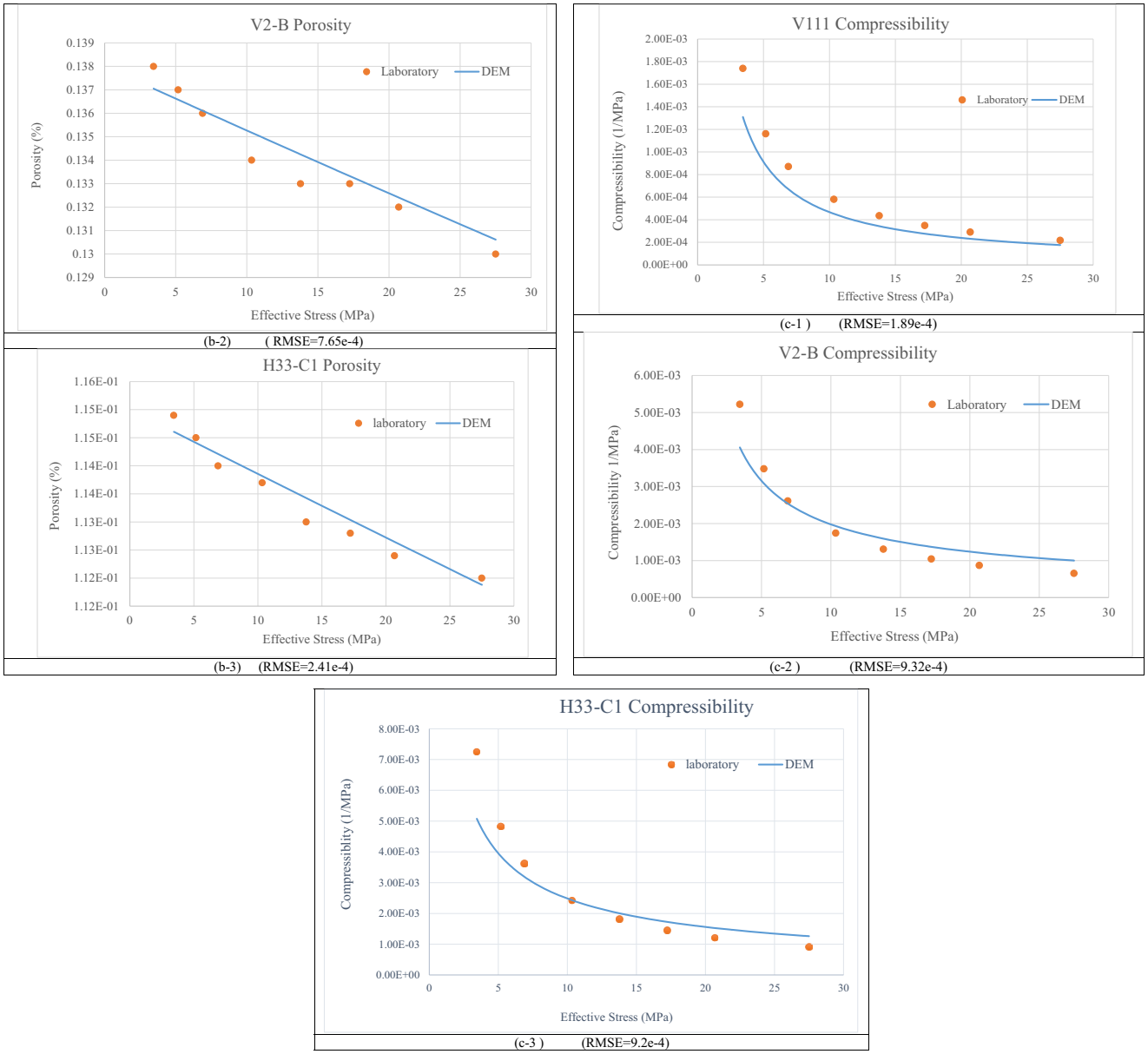

Fig. 5 continued.

Fracture permeability behaves differently between 0 and 70 and 70 and 90 degrees. In a horizontally fractured sample, fractures do not cut the sample end; there is no route for fluid drainage and pressure reduction through fractures, so the fluid is only discharged from the matrix. In other words, horizontal fractures are compressed due to applied stresses on the fracture surface. Therefore, there is no significant stress sensitivity of porosity and permeability. In the experimental investigation, although the V2 specimen has dominant horizontal fractures, the presence of some oblique and vertical fractures makes fluid discharge possible but does not prove the orientation effect properly.

Applied stresses on fracture surface have soared fracture pore pressure, while pressure drop only has happened on fractures that fluid discharged. In 50- to 90-degree fractured samples, further joints cut sample end, and more fluid discharge occurred. Therefore, by increasing fracture angle from the horizon and approaching vertical position, normal stresses on fracture surface increase, resulting in pressure drop, permeability reduction, and increasing fracture compressibility.

As discussed earlier, the CMS-300 has the capability of applying hydrostatic loads; therefore, numerical simulation is in hydrostatic condition. The loads are applied in the range that the specimens are in the elastic phase, and no failure occurs through porous medium and fractures. It means that fracture deformation is dominated by compression and shear deformation and dilation are neglected. In this simulation, in vertical and semi-vertical fractures (80 and 90 degrees), slightly shear displacement has occurred in fractures close to the

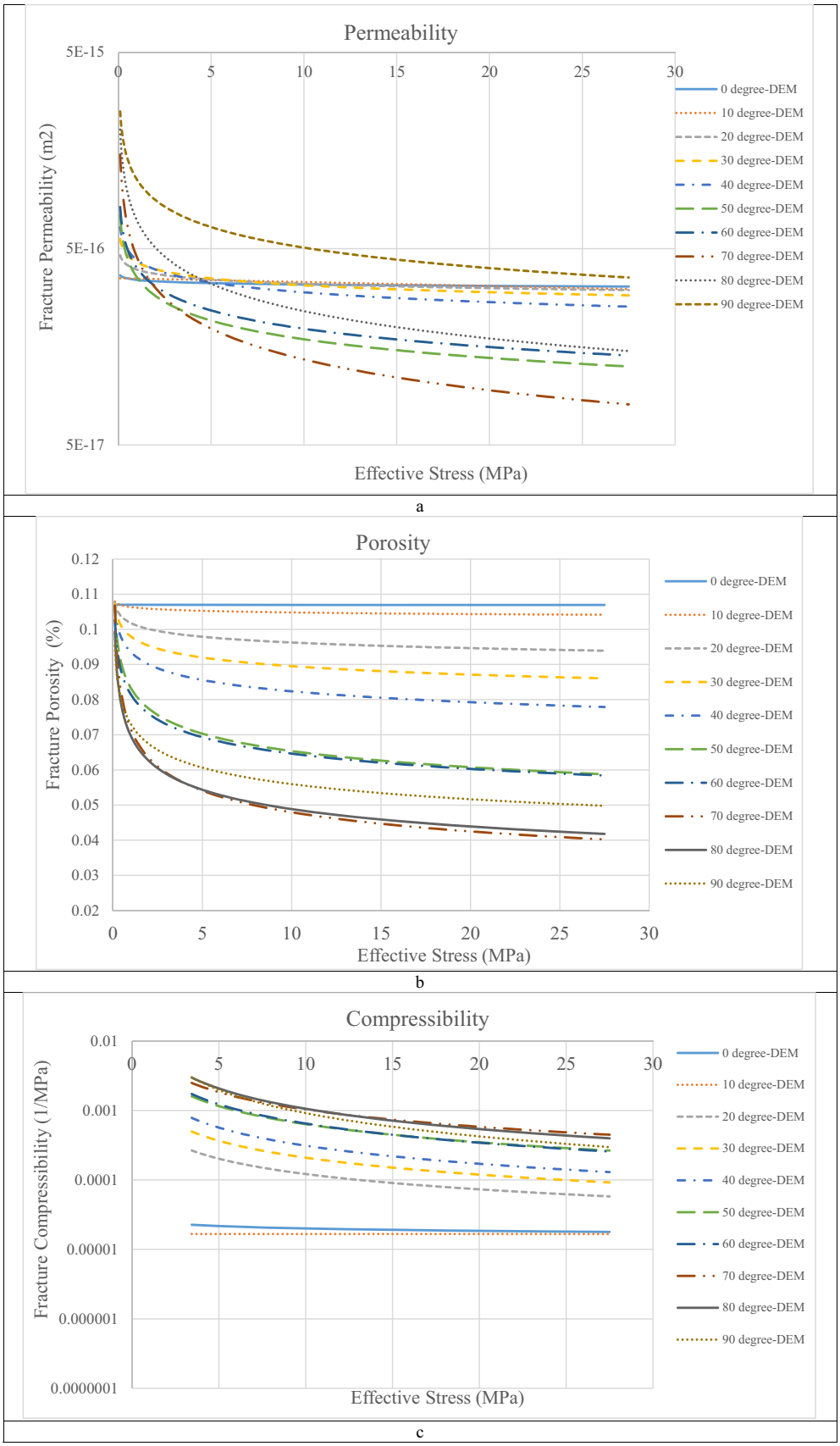

Fig. 6 Estimated values of **a** fracture permeability, **b** porosity, and **c** compressibility relative to the effective stress in 0- to 90-degree oriented fractured specimens

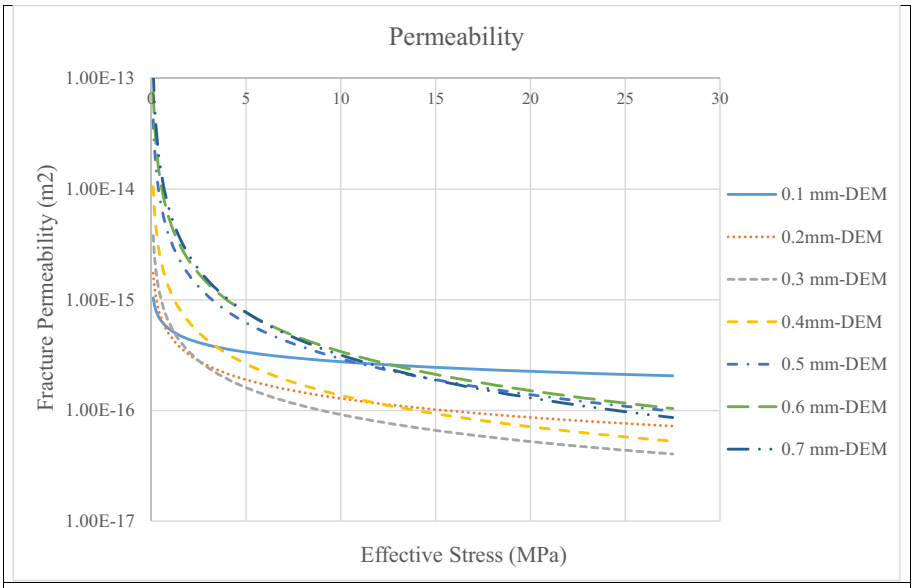

a

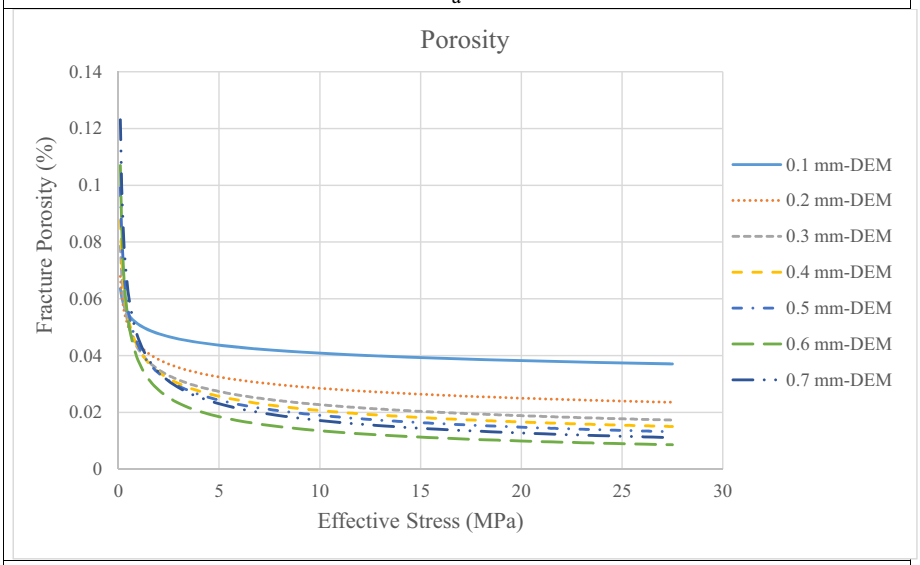

b

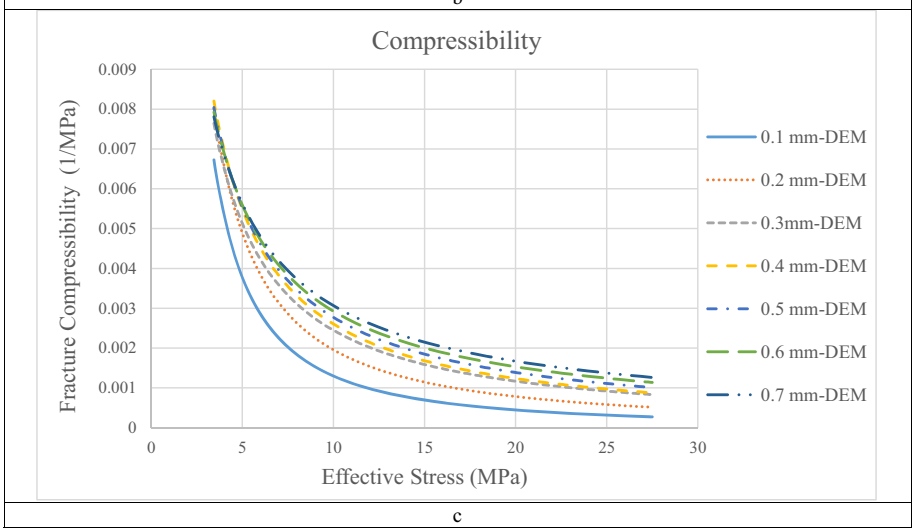

c

Fig. 7 Estimated values of **a** fracture permeability, **b** porosity, and **c** compressibility relative to effective stress in samples with two 90-degree-oriented fractures and 0.1-, 0.2-, 0.3-, 0.4-, 0.5-, 0.6-, and 0.7-mm opening

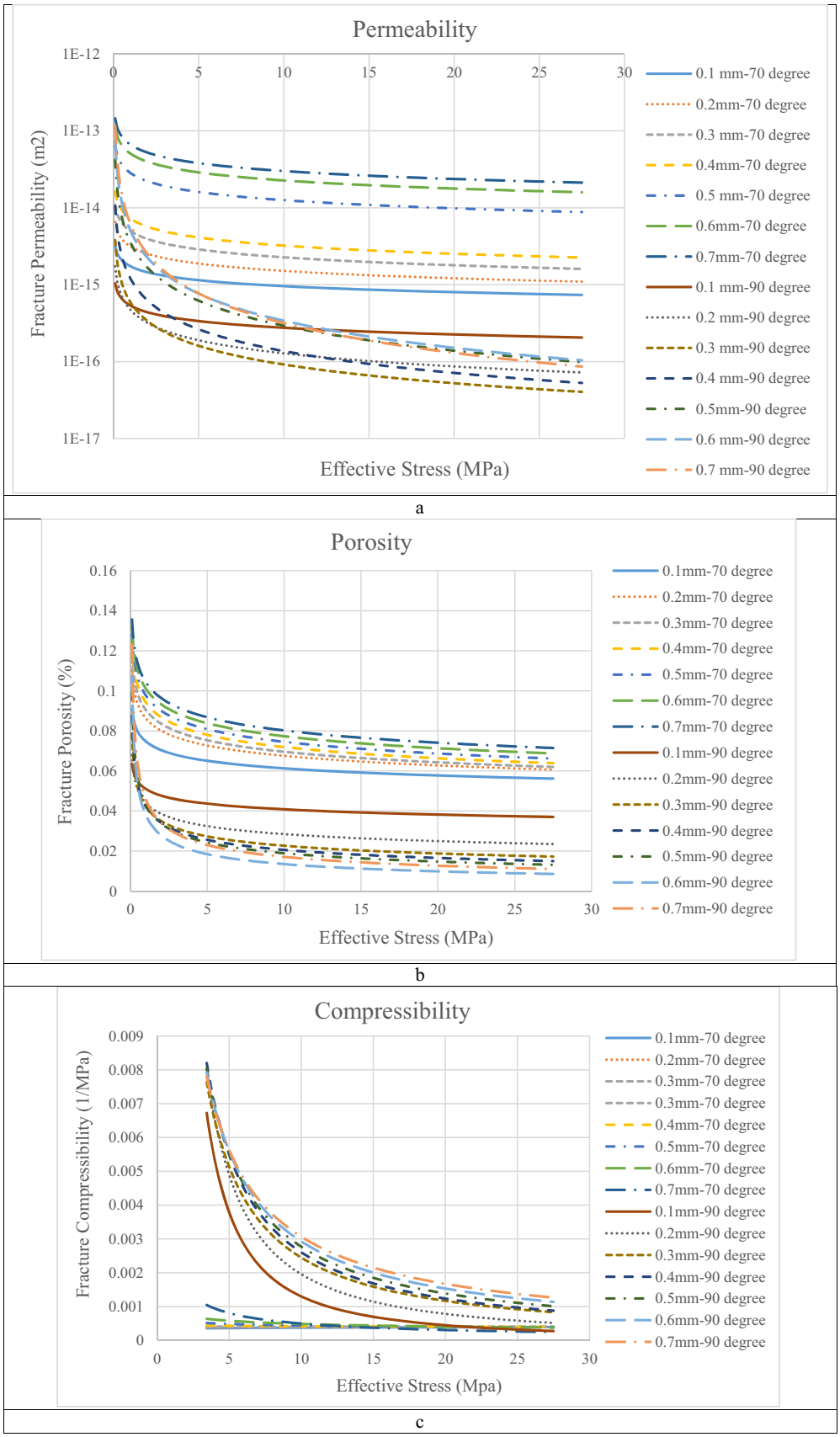

Fig. 8 Estimated values of **a** fracture permeability, **b** porosity, and **c** compressibility relative to effective stress in 90- and 70-degree-oriented fractures and 0.1-, 0.2-, 0.3-, 0.4-, 0.5-, 0.6-, and 0.7-mm opening with two fractures

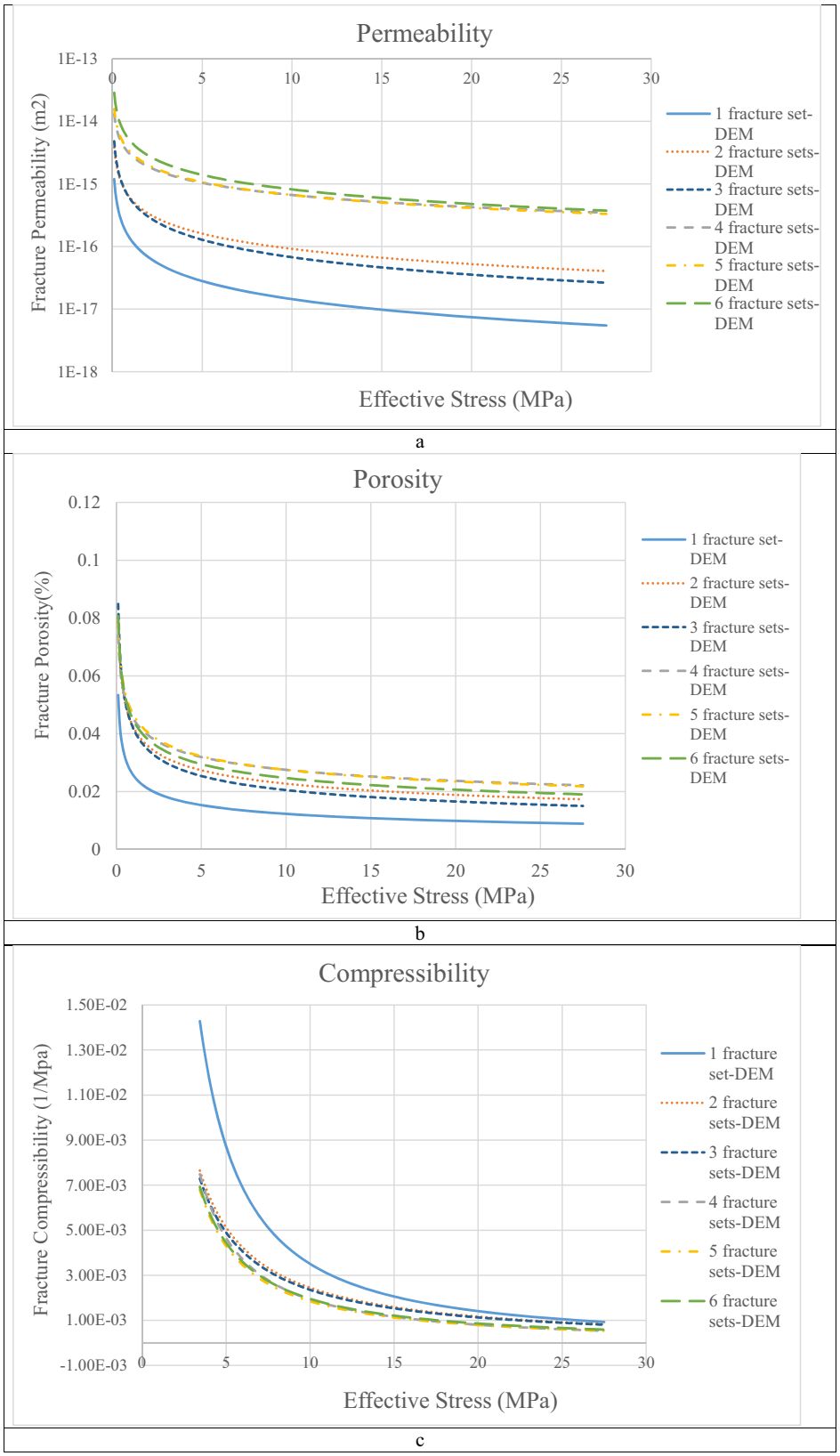

Fig. 9 Estimated values of **a** fracture permeability, **b** porosity, and **c** compressibility relative to effective stress in samples with two 90-degree-oriented fractures, 0.3-mm opening, and 1 to 6 fracture densities

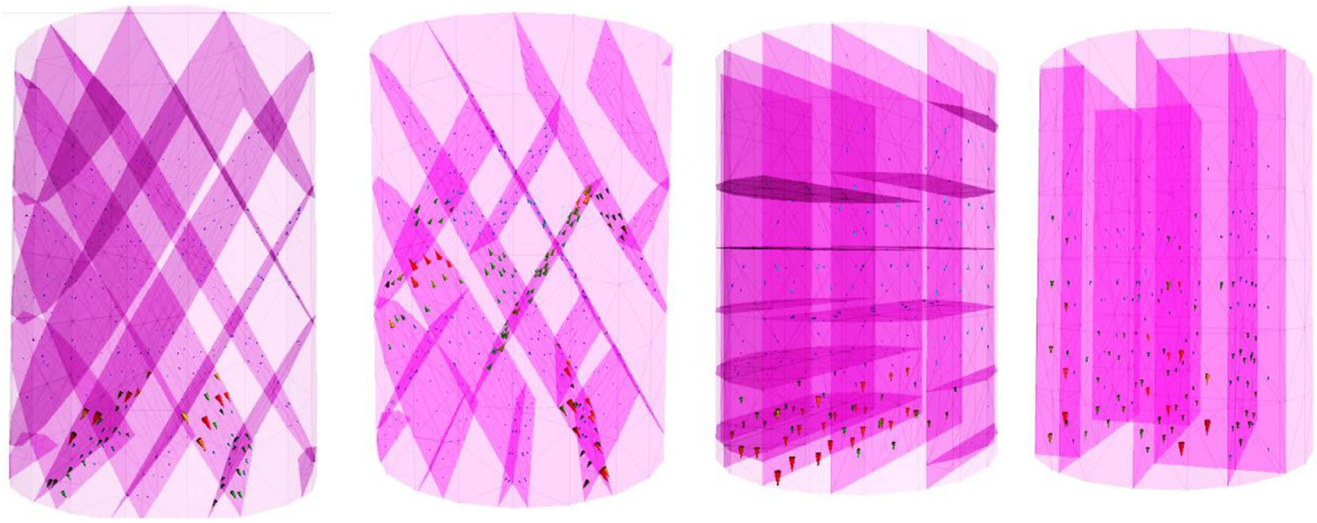

Fig. 10 Discharge vectors in **a** 60- and 120-degree orthogonally intersected fractures with 100% persistency, **b** 60- and 120-degree orthogonally intersected fractures with 50% persistency, **c** vertically and horizontally intersected fractured with 50% persistency, and **d** two vertically intersected fractures with 50% persistency

boundaries as the result of boundary conditions. Shear displacement decreases fracture closure and maintains fracture permeability and porosity. Shear deformation is linear and shear stiffness of the joint is constant.

Fracture opening effect on permeability, porosity, and compressibility

In this section, the effects of fracture opening in samples with two vertical fractures, 14 mm spacing, and 0.1, 0.2, 0.3, 0.4, 0.5, 0.6, and 0.7 mm opening are studied.

Fracture permeability, porosity, and compressibility concerning effective stress are shown in Fig. 7. The results indicate that fracture opening in vertical joints enhances discharge rate, making pore pressure drop, and increases stress-dependent permeability and porosity. While in fractures by 0.7-mm opening, the stress sensitivity of permeability and porosity is 88 and 4 times greater than 0.1-mm fracture opening. That is observed in the H33 sample, which has considerable opening than other specimens. In unpacked fractures with a large opening, the joints are rarely connected, and there is more space for fracture deformation. As a result, they simply close at the early stages of loading, and permeability reduces significantly. So during production from a low fracture opening reservoir, methods like proppant and fluid injection should be used to maintain fracture opening.

Simultaneous effect of fracture orientation and opening on permeability, porosity, and compressibility

The fracture orientation and aperture effects in vertically directed fractures have been studied in sections 4.2.1 and 4.2.2. Now, to find the dominant effect of orientation or opening on poroelastic parameters of fracture, two kinds of specimens with two parallel, 70- and 90-degree fractures; 0.1-, 0.2-, 0.3-, 0.4-, 0.5-, 0.6-, and 0.7-mm openings; and 14-mm spacing are explored. The results are shown in Fig. 8.

First, by considering the effect of fracture direction, it is understood that there are higher compressibility and lower porosity and permeability in 90 degrees fractured sample. Since there is more stress on the fracture surface, more pressure drop and fluid discharge occurred.

It should be noted that studied samples in this section have two fractures located in the middle of the sample and the shear displacement effect through 90-degree fractures (discussed in section 4.2.1) has not emerged.

In both 90- and 70-degree-oriented fractures, the more fracture opening is, the more initial permeability and porosity are.

Stress sensitivity of permeability and porosity in a 90-degree specimen increased by arising fracture opening. On the other hand, stress sensitivity of permeability in 70 degrees fractured sample is the same in almost all fracture apertures. Also, fracture compressibility values are very close to each other in different openings. Therefore, fracture aperture changes in 90-degree-oriented fractures are more significant.

Fracture density effect on permeability, porosity, and compressibility

In this section, the effects of fracture density in specimens with one to six vertical fractures, same spacing, and 0.3-mm opening are studied. Fracture permeability, porosity, and compressibility variation concerning effective stress are shown in Fig. 9.

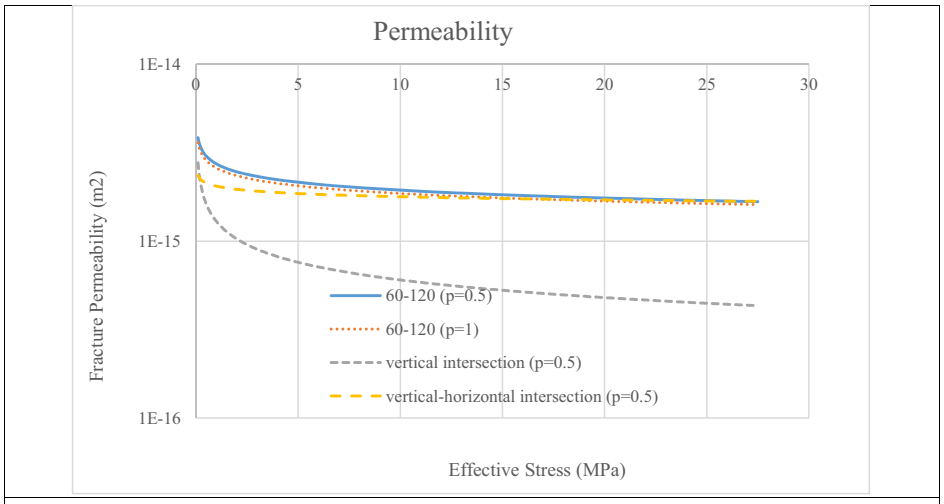

a

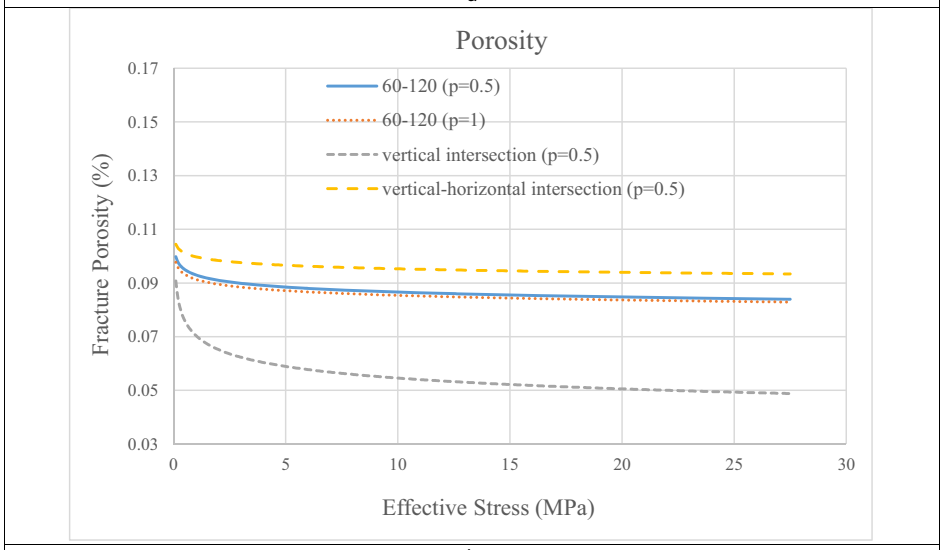

b

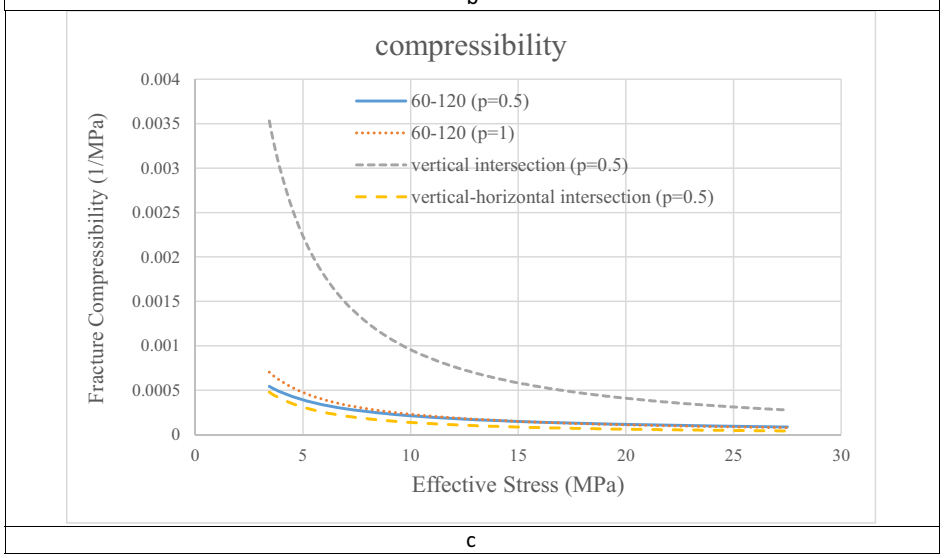

c

Fig. 11 The comparison of estimated values of **a** fracture permeability, **b** porosity, and **c** compressibility relative to effective stress in samples with 60 and 120 degree intersected fractures in fully ($p = 1$) and 50% ($p = 0.5$) persistency, vertically and horizontally intersected fractures, and two vertically intersected fractures with 50% persistency ($p = 0.5$)

The sample's compressibility value with one fracture is significantly greater than the sample with more than one fracture. Since the dominant mechanism in fracture closure is applied stresses on the fracture surface, by increasing the number of fractures, normal stresses on each fracture are divided and decreased in comparison to one fracture. The stress sensitivity of permeability and porosity in one fractured sample is 1.6 and 1.2 times greater than the specimen with six fractures. In other words, there is more stress concentration in a low fractured density medium and causes more fracture closure. In high fracture densities, fracture compressibility values become close to each other such as continuous fractured media.

In some cases, increasing the number of fractures does not affect fracture compressibility, while the compressibility of fractures and matrix coincides simultaneously in a fractured network. So, special measures should be taken to prevent pressure drop and recovery reduction in the production stage from low-density fractured reservoirs. In general, low fracture density reservoirs are more susceptible to compression and should be considered more.

For example, in laboratory specimens, the H33 sample has less fracture density, while the highest stress sensitivity of permeability is observed in this specimen. It is worth mentioning that there are several factors in laboratory specimens that simultaneously affect the results.

Simultaneous effect of fracture orientation, persistency, and intersections on permeability, porosity, and compressibility

Depending on fracture orientation and position, fracture persistency can change poroelastic parameters.

In this regard, two sets of orthogonal fractures (60 and 120 degrees) in two states of 100% and 50% persistency ($p = 1$ and 0.5 respectively), horizontally and vertically intersected fracture sets ($p = 0.5$), and two vertically intersected fracture sets ($p = 0.5$) are modeled and analyzed. As discharge vectors are shown in Fig. 10, horizontal and oblique fractures are like flow barriers, especially when there are not persisted, so the direction of fluid flow is changed alternatively in intersected fractures. Changes in fluid direction prevent fluid from directing to the production well, and in some cases, fluid has trapped in the reservoir. Meanwhile, the direction of dominant discharge vectors in two vertically intersected fractures is downward, which causes more pressure drop and fluid discharge. It is highlighted that in the designing stage, the direction of dominant fractures for further production should be considered.

Permeability, porosity, and compressibility changes in the specimens mentioned above are shown in Fig. 11. The comparison of persistency in 60- and 120-degree orthogonal fractures demonstrates that, in the fully persisted sample, as the flow path is continuous and open for fluid depletion, more pressure drop occurs that induce more compression on fractures, thereby reducing fracture aperture and hydraulic conductivity. In 50% persisted fractures, the fluid is trapped in the fracture network, so it cannot easily be driven by the contraction of fracture volume and fluid expansion. On the other hand, there is more pressure depletion in two vertically persisted fractures despite 50% persistency. It means that pore pressure drop increases while the fracture intersects the well vertically as under depletion fracture permeability values continue to decline and compressibility increases.

Conclusion

In this research paper, the stress dependence of permeability, porosity, and compressibility of fractured carbonate rocks is investigated by laboratory experiments and numerical simulations. Fractured and non-fractured specimens were tested, and the effects of fracture parameters are analyzed. Due to complexity of the natural samples and the combination of several influential factors, sensitivity analyses were carried out in order to investigate the importance of each parameter utilizing numerical simulations. The obtained results in fractured porous media can then extend to fractured reservoirs with some modifications.

The results from the laboratory experiments showed that the stress sensitivity of permeability and compressibility are more in fractured carbonate porous media in comparison to non-fractured ones. Fracture stress-dependent permeability is considerably larger than matrix values. On the other hand, by applying stresses, fracture porosity is reduced in a smooth slope. It means that fracture porosity is not so sensitive to stress changes.

It is also shown that fracture orientation is the most critical parameter in production of hydrocarbon from naturally fractured reservoirs. More fluid is produced from the horizontal fractures that intersect the well vertically. Deviation of the joint from the vertical position (respect to well), even to a small extent, has a significant impact on productivity.

There is more stress concentration on fractures in a low fractured density medium and causes more fracture closure. In high fracture densities, fracture compressibility values become close to each other. High fracture density is such a continuous fractured media. By increasing the number of fractures, the compressibility of fractures and matrix occurs simultaneously in a fractured network.

In reservoirs with open fractures and no filling, more pressure drop and compressibility occurred in the early stages of production. Therefore, different injection methods should be used to keep the joints open. The presence of some filling materials can act as a natural proppant that keeps fractures open.

The analysis also showed that the intersected fractures that are inclined verticality to the production well contribute more in the production even if they have not

fully persisted. Horizontal joints (respect to well) act as barriers that prevent fluid passage and therefore reduce productivity.

Finally, the experimental results which consider the total variation of matrix and fractures and by using analytical relationships, the permeability, porosity, and compressibility of fractures were obtained. Hence, the fowling general equation is developed to calculate the compressibility of the matrix: $C_{\mathrm{pc,m}} = -\frac{p}{k_{\mathrm{f}}} - \left[\frac{\alpha}{K}\left(P - \frac{pK\varnothing}{\alpha K_{\mathrm{f}}}\right)\right] / \nabla P$.

Notations The following symbols are used in this paper:

$u_h$joint normal displacement
u_{h0}joint aperture in zero normal stress
Δu_nnormal displacement of fracture
Ct_ffracture compressibility
$\phi_f$fracture porosity
$K_f$fracture permeability
ϕ_{fi}initial fracture porosity
K_{fi}initial fracture permeability
Ppiinitial pore pressure
Ppcurrent pore pressure
*b*current fracture width
biinitial fracture width
ΔV_fvariation of fluid volume
$K_f$fluid bulk modulus
ζvariation of fluid content
*P*applied confining pressure
*p*pore pressure
*B*Skempton pore pressure coefficient
$C_{\mathrm{pc\ (f)}}$fracture compressibility
$C_{\mathrm{pc(m)}}$matrix compressibility
αBiot coefficient
$K_p$bulk modulus for the pore volumetric strain
*K*permeability

References

Abass HH, Ortiz I, Khan MR, Beresky JK, Armaco S, Sierra L, Halliburton (2007) "Understanding stress dependent permeability of matrix, natural fractures, and hydraulic fractures in carbonate formations", Society of Petroleum Engineers. SPE 110973(May):1–8

Aguilera R (1999) Recovery factors and reserves in naturally fractured reservoirs. J Can Pet Technol 38(7):15–18

Aloki Bakhtiari H, Moosavi A, Kazemzadeh E, Goshtasbi K, Esfahani MR, Vali J (2011) The effect of rock types on pore volume compressibility of limestone and dolomite samples. Geopersia 1(1):37–82

Bagherzadeh P, Goshtasbi K, Kazemzadeh E (2021) Stress-dependence of the permeability, porosity, and compressibility of fractured carbonate rock. J Porous Media 24(5):21–45

Carvajal J, Saavedra N, Calderon Z (2010) Stress effect on compressibility of weakly anisotropic micro-fractured rocks a study case on Colombian foothills tight sandstones. 44th U.S. Rock Mechanics Symposium and 5th U.S.-Canada Rock Mechanics Symposium, June 27–30

Chacon, A. (2006) Effect of pressure depletion on hydrocarbon recovery in naturally fractured reservoirs", a dissertation submitted in partial fulfillment of the requirements for the degree of doctor of philosophy, Norman, Oklahama

Chen D, Pan Z, Ye Z (2015) Dependence of gas shale fracture permeability on effective stress and reservoir pressure: model match and insights. Fuel 139:383–392

Chen D, Pan Z, Ye Z, Hou B, Wang D, Yuan L (2016) A unified permeability and effective stress relationship for porous and fractured reservoir rocks. J Nat Gas Sci Eng 29:401–412

Detournay E, Cheng A (1993) Fundamental of poroelasticity. In: Fairhurst C (ed) Comprehensive Rock Engineering: Principles, Practice and Projects, Vol. II, Analysis and Design Method. Pergamon Press, pp 113–171

Dong JJ, Hsu JY, Wu WJ, Shimamoto T, Hung JH, Yeh EC, Sone H (2010) Stress-dependence of the permeability and porosity of sandstone and shale from TCDP Hole-A. Int J Rock Mech Min Sci 47(7): 1141–1157

Dwi HF, Natalia S, Castillo D (2007) The effect of pressure depletion on geomechanical stress and fracture behavoir in gunung kembang field. In: In procceding of indonesion petroleum Association. Annual Convention and Exhibition, Thirty-first

Ghanizadeh A, Gasparik M, Amann-Hildenbrand A, Genesterblum Y, Krooss BM (2014) Experimental study of fluid transport processes in the matrix system of the European organic-rich shales: I. Scandinavian Alum Shale. Mar Pet Geol 51

Haifeng Z, Jun S, Erfei M, Hang C, Guohua L (2015) Scale model of stress sensitivity for fractured low permeability reservoirs. Proceedings, Fortieth Workshop on Geothermal Reservoir Engineering Stanford University, Stanford, California, SGP-TR-204

Hall HN (1953) Compressibility of reservoir rocks. Pet Trans AIME 198: 309–311

Harari Z, Shu-Teh W, Salih S (1995) Pore-compressibility study of Arabian carbonate reservoir rocks. SPE Form Eval 10(4):207–214

Itasca CG (2013) 3DEC-User manual. Itasca ConsultingGroup, Minneapolis

Jalalh AA (2006a) Compressibility of porous rocks: Part I. Measurements of Hungarian Reservoir Rock Samples. Acta Geophys 54(3):319–332

Jalalh AA (2006b) Compressibility of porous rocks: Part II. New relationships. Acta Geophys 54(4):399–412

Liu HH, Rutqvist J, Berryman JG (2009) On the relationship between stress and elastic strain for porous and fractured rock. Int J Rock Mech Min Sci 46(2):289–296

Lun ZL, Yefei C, Zhengfu N, Xuelin W, Lifang L, Xi C (2013) Stress sensitive experiments for abnormal overpressure carbonate reservoirs: a case from the Kenkiyak fractured-porous oil field in the littoral Caspian Basin. Pet Explor Dev 40(2):208–215

Luo J, Stevens R (1996) Micromechanics of randomly oriented ellipsoidal inclusion composites Part II: elastic moduli. J Appl Phys 79(12): 9057–9063

MA Y, Pan Z, Zhong N, Connell LD, Down DI, Lin W, Zhang Y (2016) Experimental study of anisotropic gas permeability and its relationship with fracture structure of Longmaxi Shales, Sichuan Basin, China. Fuel 180:106–115

Moosavi SA, Goshtasbi K, Kazemzadeh E, Bakhtiari HA, Esfahani MR, Vali J (2014) Relationship between porosity and permeability with stress using pore volume compressibility characteristic of reservoir rocks. Arab J Geosci 7(1):231–239

Newman GH (1973) Pore-volume compressibility of consolidated, friable, and unconsolidated reservoir rocks under hydrostatic loading. J Pet Technol 25(2):129–134

Pan Z, Ma Y, Connell LD, Down DI, Camilleri M (2015) Measuring anisotropic permeability using a cubic shale sample in a triaxial cell. J Nat Gas Sci Eng 26:336–344

Pinzon CL, Chen H, Teufel LW (2000) Complexity of well testing analysis of naturally-fractured gas-condensate wells in Colombia. Paper SPE 59013 presented at the 2000 SPE international petroleum conference and exhibition, Mexico

Ross DJK, Bustin RM (2008) Characterizing the shale gas resource potential of Devonian-Mississippian strata in the Western Canada

sedimentary basin: Application of an integrated formation evaluation. AAPG Bull 92(1):87–125

Soeder DJ (1988) Porosity and permeability of Eastern Devonian gas shale. SPE Form Eval, (March), pp 16–24

Tan Y, Pan Z, Feng XT, Zhang D, Connell LD, Li S (2019) Laboratory characterization of fracture compressibility for coal and shale gas reservoir rocks: a review. Int J Coal Geol 204:1–17

Tan Y, Pan Z, Liu J, WU, Y., Haque, A., & Connell, L. D. (2017) Experimental study of permeability and its anisotropy for shale fracture supported with proppant. J Nat Gas Sci Eng 44:250–264

Tao Q, Ehlig-economides CA, Ghassemi A (2009) Investigation of stress-dependent fracture permeability in naturally fractured reservoirs using fully coupled poroelastic displacement discontinuity model." In SPE annual conference and exhibition. USA

Wang Z, Jin X, Wang X, Sun L, Wang M (2016) Pore-scale geometry effects on gas permeability in shale. J Nat Gas Sci Eng 34:948–957

Zhang G, Ranjith PG, Liang W, Haque A, Perera MSA, Li D (2019) Stress-dependent fracture porosity and permeability of fractured coal: an in-situ X-ray tomography study. Int J Coal Geol 213: 103279

Zheng Z (1993) Compressibility of porous rocks under different stress conditions. Int J Rock Mech Min Sci Geomech Abstr 30(2):1181–1184

Zheng J, Ju Y, Liu H, Zheng L, Wang M (2016) Numerical prediction of the decline of the shale gas production rate with considering the geomechanical effects based on the two-part Hooke's model. Fuel 185:362–369

Zhou J, Zhang L, Li X, Pan Z (2019) Experimental and modeling study of the stress-dependent permeability of a single fracture in shale under high effective stress. Fuel 257:116078

Zimmerman W, Somerton WH, King MS (1986) Compressibility of porous rock. J Geophys 91(6):765–777